PROCEEDINGS, 48th Workshop on Geothermal Reservoir Engineering
Stanford University, Stanford, California, February 6-8, 2023
SGP-TR-224

Comparison of Modeling Results with Data Recorded During Field Stimulations at Utah FORGE Site

Pengju Xing[1], Branko Damjanac[1], Zorica Radakovic-Guzina[1], Maurilio Torres[1], Aleta Finnila[2], Robert Podgorney[3], Joseph Moore[4], John McLennan[5]

1 Itasca Consulting Group, Inc., Minneapolis, MN, USA
2 Golder Associates USA, Inc., Redmond, WA, USA
3 Idaho National Laboratory, Idaho Falls, ID, USA
4 Energy & Geoscience Institute, University of Utah, Salt Lake City, UT, USA
5 Department of Chemical Engineering, University of Utah, Salt Lake City, UT, USA

Keywords: Hydraulic stimulation, microseismicity, numerical simulation, Enhanced Geothermal System, Utah FORGE

ABSTRACT

Three stages of stimulation were carried out near the toe of well 16A(78)-32 at Utah FORGE site. Previously, before the actual field stimulations, predictions of stimulation effects were conducted using numerical models. Modeling results were compared to field data in three aspects: 1) injection pressure history, 2) spatial distribution of microseismic events, and 3) b-values of microseismic events.

After the comparison we find that the models with weak, frictional and permeable DFN yield the best match for all three stages. All three stages appear to include combinations of hydraulic fracturing and stimulation of DFN. DFN leakoff seems to dominate the response in Stages 1 and 2, which is logical considering the use of slick water. Stage 3, which was stimulated with xlink fluid, is dominated by hydraulic fracture propagation. The injection pressure history for Stage 1 matches well with the field data. Injection pressure histories for Stages 2 and 3 (cased completion with perforations) were not matched well at early period potentially due to complex evolving geometries and processes in the well near field are not included in this model. For all the three stages, the extents of microseismicity events in the models match the field data. The b values of the microseismic events from the models ranging from 2.3 to 2.4 are very close to those obtained from the field for all three stages.

1. INTRODUCTION

In April of 2022, three stages of stimulation were carried out near the toe of well 16A(78)-32 at Utah FORGE site (McLennan et al., 2023). During the field stimulations, pumping pressure, pumping rate, and microseismic events were recorded. Previously, before the actual field stimulations, predictions of stimulation effects were conducted using numerical models. The models, which explicitly represent discrete fractures, used different discrete fracture network (DFN) strengths (from weak and initially permeable to strong and initially impermeable) and different DFN geometrical realizations (due to stochastic nature of the DFN). The results of these models were documented by Xing et al., 2022. In this study, the modeling results were compared with the data collected from three stimulation stages in three aspects: 1) injection pressure history, 2) spatial distribution of microseismic events, and 3) b-values of microseismic events.

First, the field stimulations are briefly introduced. Then, the numerical models and relevant parameters are reviewed. Finally, the results from the numerical models are compared to the field data.

2. FIELD STIMULATIONS

The locations of the three stages are illustrated in Figure 1. Stage 1 was conducted in the openhole section at the toe, and Stages 2 and 3 were conducted from perforation clusters in the cased section. Figure 2 shows the pumping rates and surface pressure histories during the stimulations of the three stages. Table 1 summarizes the pumping information for the three stages. For Stages 1 and 2, slickwater was used while xlink gel was used in Stage 3.

The stimulation was monitored by geophones in multiple offset wells. The recorded and interpreted microseismic events are shown in Figure 3 and the summary is provided in Table 2.

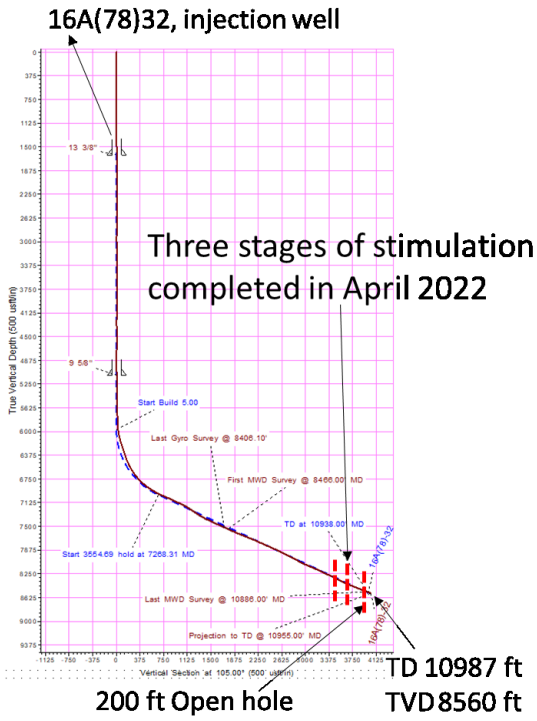

Figure 1: Locations of the three stages

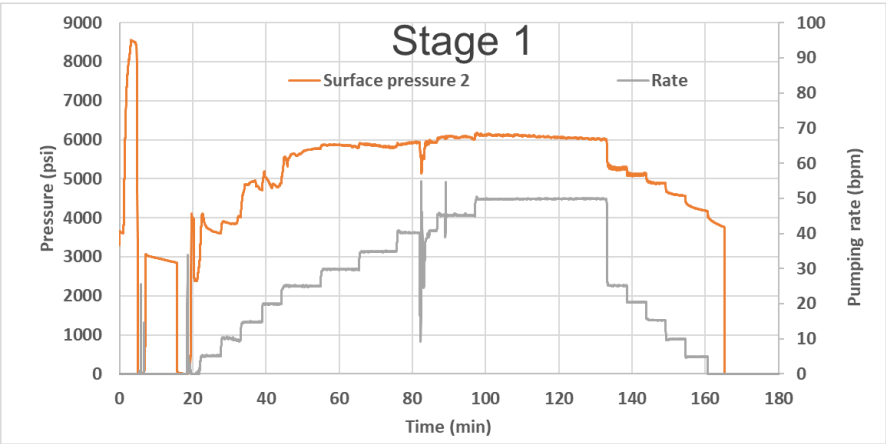

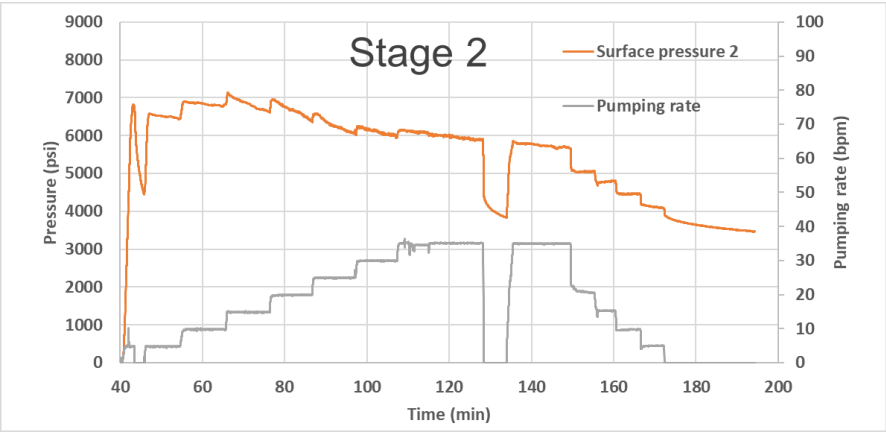

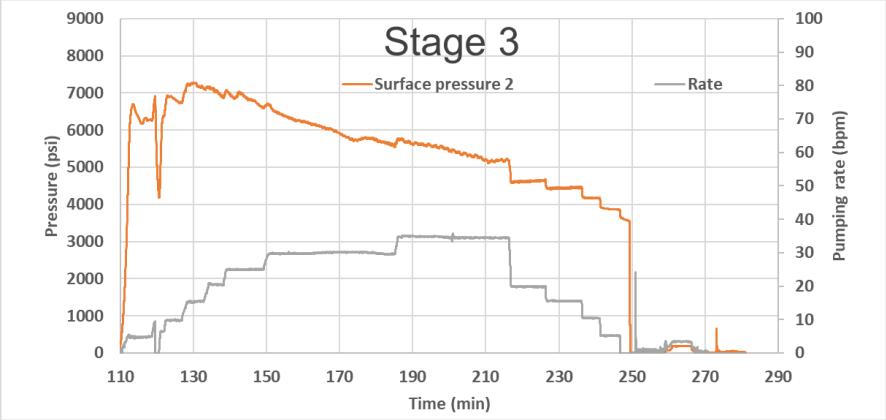

Figure 2: Pumping rates and surface pressures for the three stimulation stages.

Table 1. Field pumping information for the three stages stimulation

Stage No.	Pumping fluid	Maximum pumping rate (bpm)	Pumped volume (bbl)	Completion	TVD (ft)
1	Slickwater	50	4261	Openhole	8490
2	Slickwater	35	2777	Cased	8410
3	xlink gel	35	3016	Cased	8224

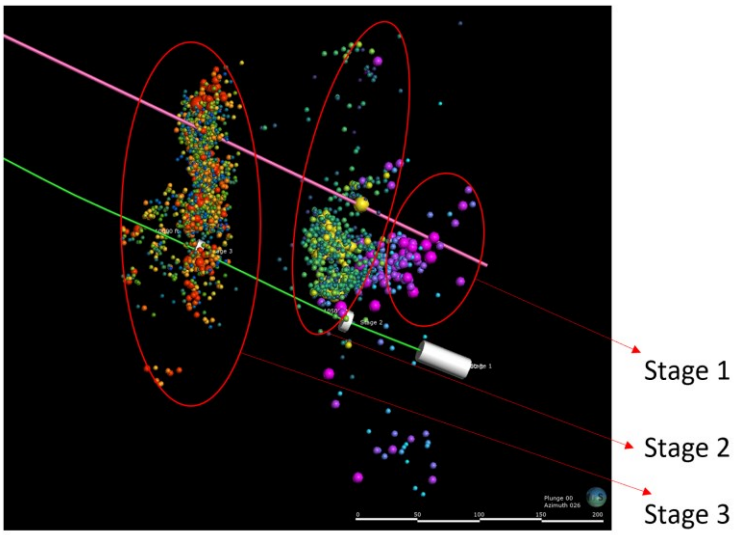

Figure 3: Recorded and interpreted microseismic events. Image is from the Utah FORGE earth model, created by Hari Neupane at INL using Leapfrog Geothermal.

Table 2. Numbers and maximum magnitudes of recorded events during stimulation.

Stage No.	Number of events detected	Maximum magnitude
1	211	0.04
2	948	- 0.33
3	1432	0.52

3. NUMEIRCAL MODELS

The simulations were conducted using a lattice-based code, XSite^{TM} (Itasca, 2020), which simulates fully coupled hydro-mechanical processes. The numerical models are well documented in Xing et al., 2022 (GRC 2022). The key parameters are restated here.

The material properties and initial stress conditions used by the numerical model are listed in Table 3. In this study, three different DFN realizations (generated using different random number generation seeds) are considered. Discrete stochastic fractures provided in the DFNs have radius values in the 10 to 150 m range and orientations matching the mean values of the four fracture sets identified from FMI logs (Finnila et al., 2021). Longer natural fractures have larger initial apertures. Two different DFN styles are considered: a permeable and frictional DFN, and a "strong DFN". As shown in Table 4, for the permeable and frictional DFN, cohesion and tensile strength are zero, initial hydraulic apertures of the fractures range from 50 to 190 μm, and initial permeability is based on the initial hydraulic apertures. For the strong DFN, cohesion is 10 MPa, tensile strength is 2 MPa. The initial hydraulic apertures are in the same range as for the permeable DFN. However, the fractures are not permeable until they fail.

Table 3. Material properties and initial conditions for well 16A(78)-32 (TVD 8490 ft, 2587.8 m)

Variable		Value
Young's modulus		55 GPa (8.0×10^6 psi)
Poisson's ratio		0.26
Fracture toughness		3 MPa×m$^{1/2}$ (2740 psi×in$^{1/2}$)
Fluid viscosity	Stage 1 and 2	Newtonian fluid, 2 cp for Stage 1 and 2
	Stage 3	Power law fluid/ Newtonian fluid, 100 – 200 cp
Pore pressure		0.0093 MPa/m (0.41 psi/ft), 24.0 MPa (3481 psi)
Minimum horizontal stress		0.0174 MPa/m (0.73 psi/ft), 42.68 MPa (6190 psi)
Maximum horizontal stress		0.0189 MPa/m (0.84 psi/ft), 48.80 MPa (7078 psi)
Vertical stress		0.0243 MPa/m (1.07 ft/ft), 62.80 MPa (9108 psi)

Table 4. DFN Properties used in Numerical Model

Parameter	Permeable and frictional DFN	Strong DFN
DFN friction angle	37°	37°
DFN cohesion	0	10 MPa
DFN tensile strength	0	2 MPa
Initial aperture	50 – 190 μm	50 – 190 μm
Initial permeability	Based on initial aperture	No

The pumping schedules in the models followed the designed pumping schedules which is slightly different from the real pumping schedule conducted in the field in April 2022.

3. PRESSURE HISTORY COMPARISONS AND ANALYSIS

To compare the injection pressures predicted in the model with the field data, it is necessary to calculate the net pressure for the field stimulations. The net pressure, which is predicted by the models, was calculated from the surface pressure recorded during the stimulation using the following formula

$$p_{net} = p_{surface} + p_{hydro} - p_f - \sigma_{hmin}$$

where $p_{surface}$ is the recorded surface pressure, p_{hydro} is the hydrostatic pressure, p_f is the friction, and σ_{hmin} is the minimum horizontal pressure. p_{hydro} can be calculated from true vertical depth (TVD) and fluid density. p_f is inferred from the pumping step down data in the stimulation. σ_{hmin} is estimated as 0.78 psi/ft from DFIT test conducted at the toe (refer to Xing et al., 2021).

3.1 Stage 1

The comparison of the net pressure between simulation and field data for Stage 1 is shown in Figure 4. The right top subfigure shows the relation between friction pressure and pumping rate, which is obtained from pumping step down data of Stage 1. The net pressure history from the field was corrected by the friction pressure. The net pressure of the numerical model after 60 minutes is close to the filed data. The DFN in this model is assumed to be weak, frictional, and permeable in-situ (refer to Table 4). The right bottom subfigure shows the simulated fracture apertures (i.e., fractures with hydraulic aperture greater than 0.2 mm) after pumping.

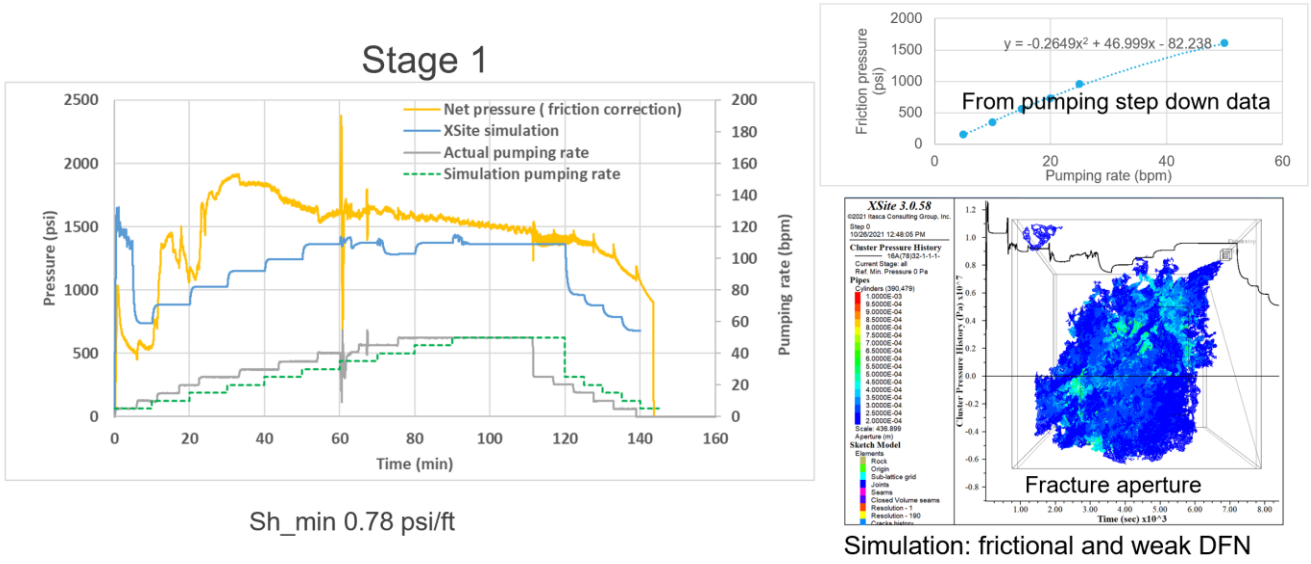

Figure 4: Comparison of the field pressure history with simulation results for Stage 1. Left: pressure history comparison; right top: friction correction for the field pressure; right bottom: simulated fracture hydraulic apertures after pumping. The DFN used in the model is assumed to be frictional, weak and permeable.

3.2 Stage 2

The comparison of the net pressure between simulation and field data for Stage 2 is shown in Figure 5. The net pressure for the field stimulation was corrected by the step-down data shown in the right top sub figure. The DFN used in the model is assumed to be frictional, weak and permeable in-situ.

The simulated net pressure after 80 minutes is close to the field data. However, there is a large discrepancy between the simulation and field data at early times, before 60 minutes of injection. The net pressure from the field data drops dramatically from 3500 psi to 1500 psi while in the model the net pressure increases gradually from 500 psi to 1000 psi. A net pressure as interpreted from the field data in the beginning of injection is unrealistically high. The high "net" pressure could be caused by the near wellbore tortuosity, which is not included in the friction pressure correction obtained from the pumping step down data because the tortuosity effect decreased with time. In Stage 2, there are 120 perforation holes in the 20-foot section (6 perforation per foot). There is possibility that fewer perforation holes were open at the beginning of injection compared to later times which leads to higher pressure loss at early times compared. The near wellbore tortuosity is more severe in the cased and perforation cluster zone compared to that in the open hole section in Stage 1.

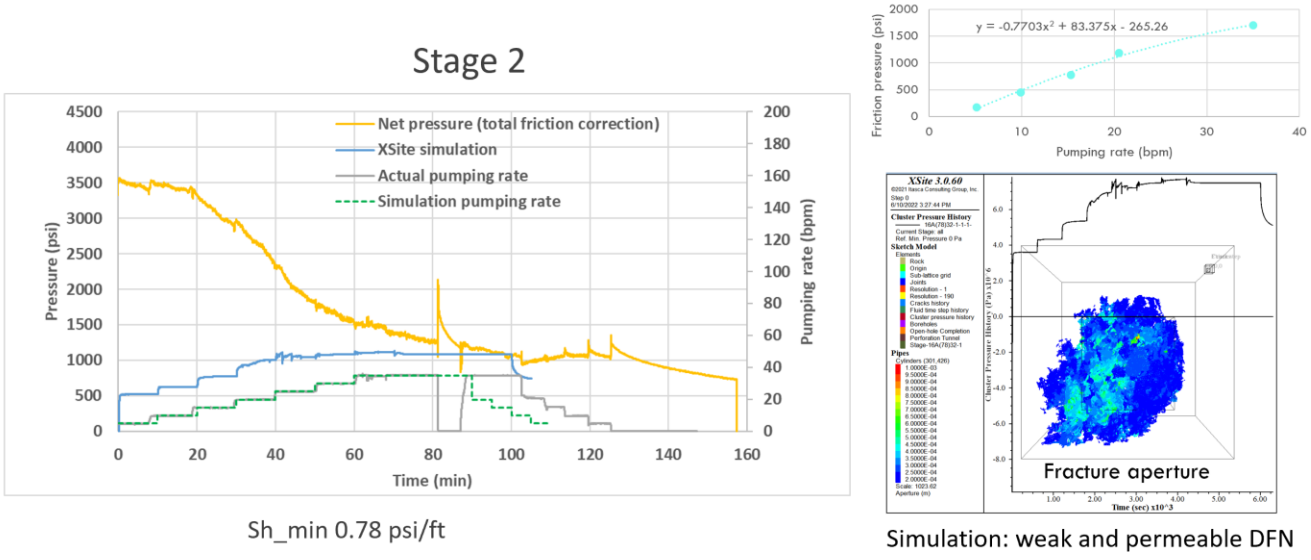

Figure 5: Comparison of the field pressure history with simulation results for Stage 2. Left: pressure history comparison; right top: friction correction for the field pressure; right bottom: simulated fracture hydraulic apertures after pumping. The DFN used in the model is assumed to be frictional, weak and permeable.

3.3 Stage 3

The comparison of the net pressure between simulation results and field data for Stage 3 is shown in Figure 6. The net pressure for the field stimulation was corrected by the step-down data shown in the right top sub figure. The DFN used in the model is assumed to be frictional, weak and initial permeable.

The simulated net pressure after 80 minutes is close to the field data. However, like in Stage 2, there is a large discrepancy between the simulation and field data before 60 minutes. The net pressure from the field data drops dramatically from 4000 psi to 1000 psi while the net pressure around 1000 – 1200 psi is predicted in the numerical model. Stage 3 is also a cased section and with perforation cluster. Therefore, the high "net" pressure in the field data could be caused by the near wellbore tortuosity.

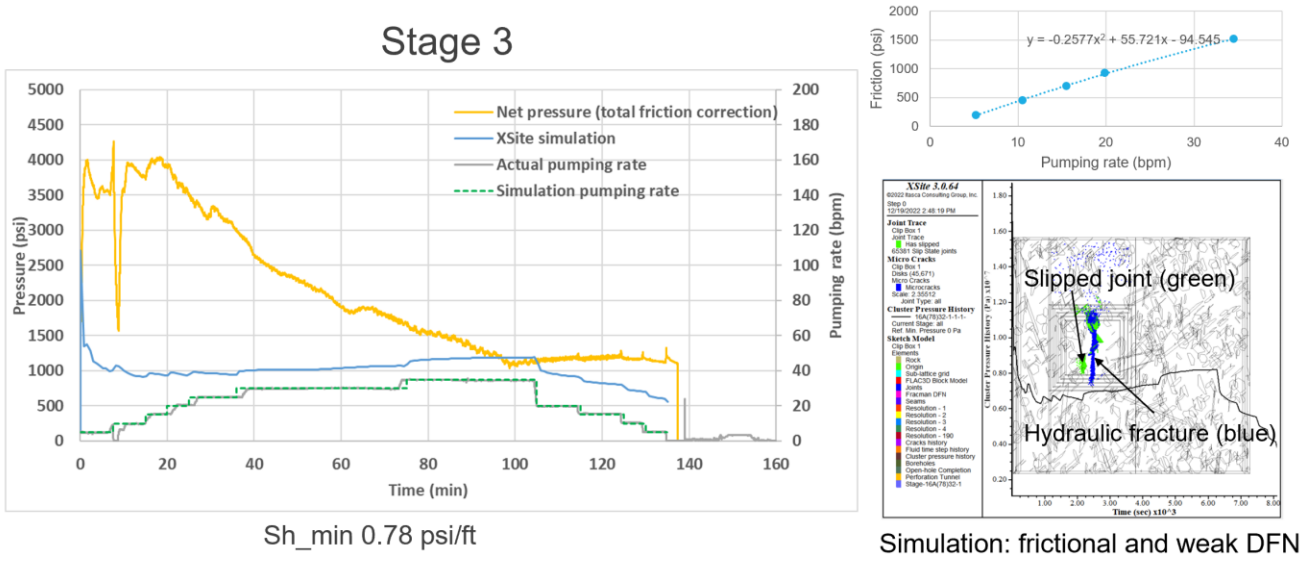

Figure 6: Comparison of the field pressure history with simulation results for Stage 3. Left: pressure history comparison; right top: friction correction for the field pressure; right bottom: simulated slipped joint and hydraulic fractures after pumping. The DFN used in the model is assumed to be frictional, weak and permeable. The viscosity in the model is 100 cP.

3.4 Summary

In all the numerical models shown above, the same DFN geometrical realization and strength (weak, frictional and permeable) were assumed. For all three stages, the stimulation is a combination of slipping of pre-existing joints and propagation of hydraulic fractures (refer to Figure 7). The extents of the slipped joints and hydraulic fractures for Stage 1 and Stage 2 are smaller than for Stage 3, which is due to the larger fluid viscosity in Stage 3. The fluid viscosity used in Stage 3 is 100 cP, while it is 2 cP in Stages 1 and 2. Larger fluid viscosity yields higher pressure, which results in more hydraulic fracture propagation and more slipping joints. The extents of DFN with apertures enhanced for Stage 1 and Stage 2 are larger than Stage 3 (refer to Figure 8), and the fracture aperture magnitude is smaller than Stage 3. That is consistent with the expectation that higher viscosity fluid yields larger fracture aperture and less leak-off.

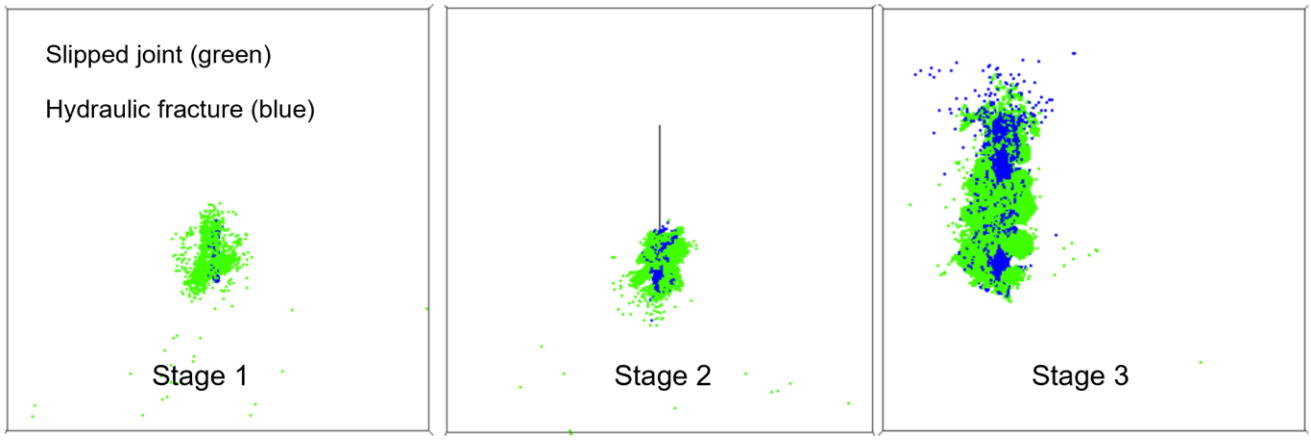

Figure 7: Slipped joints and newly created hydraulic fractures for the three stages.

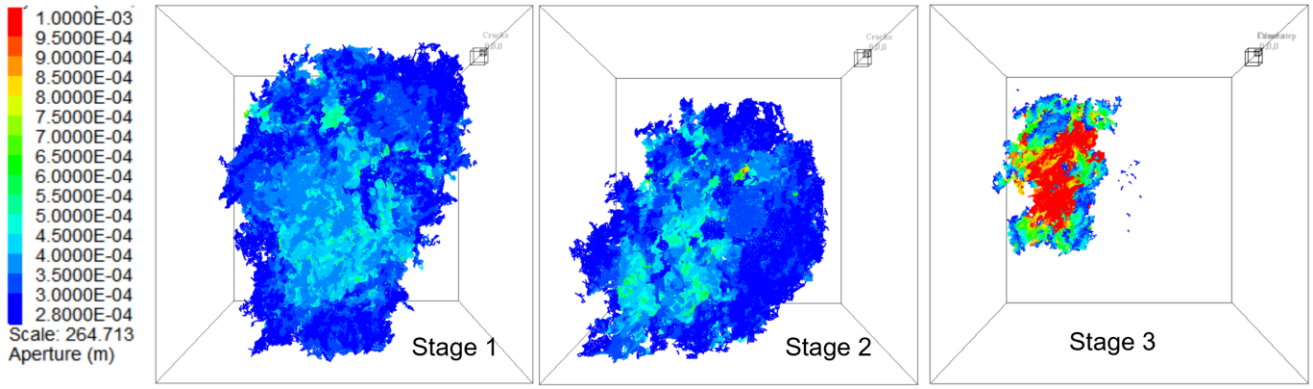

Figure 8: Hydraulic apertures of fractures at the end of pumping in the models of three stages. Only the DFN fractures with hydraulic aperture increased during the pumping are shown. The fractures with aperture less than 2.8E-4 m (maximum initial aperture) are not shown because their apertures are not increased due to fluid pumping.

4. MICROSEISMICITY EVENT COMPARISONS

In this section, the simulated microseismic events are compared with the field recorded data both by geometry extents and b value.

4.1 Stage 1

Figure 9 shows the comparison of the microseismic events generated in the numerical model and detected in the field for Stage 1. The extents and maximum magnitudes from the model match the field data. The number of events from the numerical model is much greater than the field data. As it is shown in Figure 10, the field geophones cannot detect the microseismicity magnitude smaller than – 1.5, but the magnitude can be as low as – 3.7 in the model. Nevertheless, the b value of the numerical model is 2.4, which is close to the b value of the field data, 2.3.

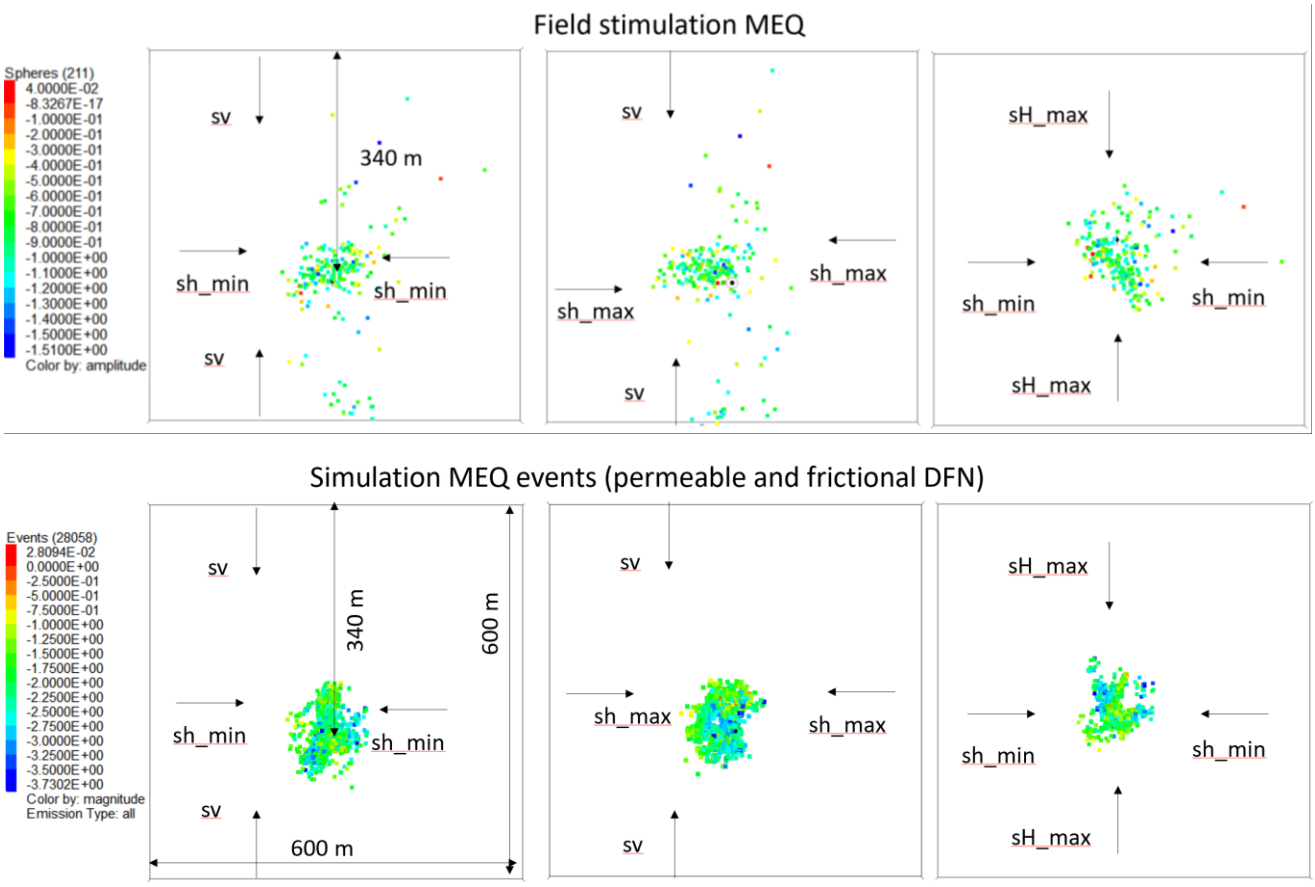

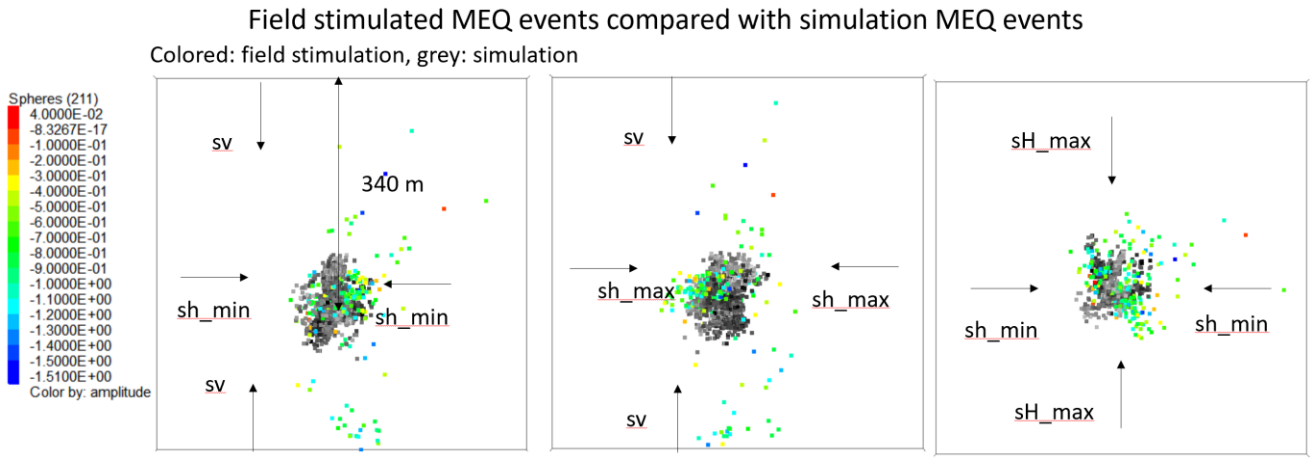

Figure 9: Comparison of the field detected microseismicity cloud with simulation results for Stage 1. Field detected maximum magnitude is 0.04, and simulation maximum magnitude is 0.03.

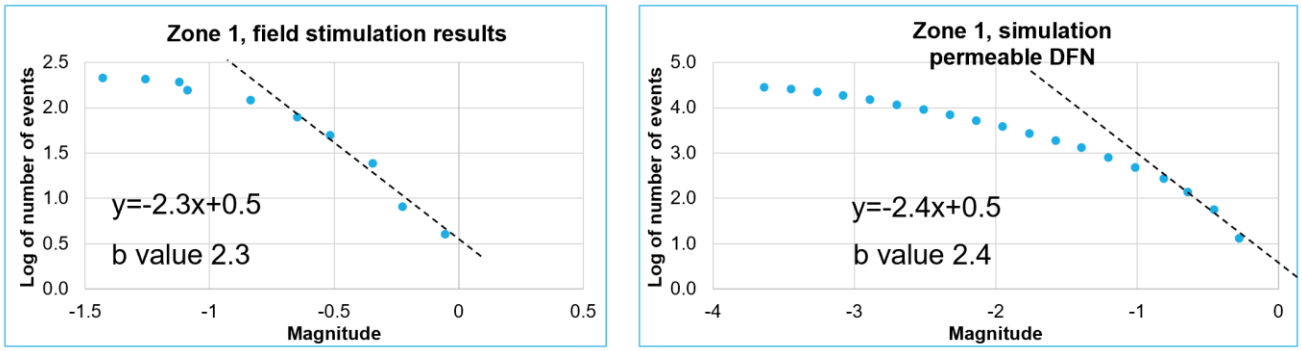

Figure 10: Comparison of the field detected microseismicity b-value with simulation results for Stage 1.

4.2 Stage 2

Figure 11 shows the comparison of the microseismic events generated in the numerical model and detected in the field for Stage 2. The extents and maximum magnitudes from the model match the field data. The number of events from the numerical model is much greater than the field data. As it is shown in Figure 12, the field geophones cannot detect the microseismicity magnitude smaller than – 2.0, but the magnitude can be as low as – 3.2 in the model. The b value of the numerical model is 2.3, which is close to the b value of the field data, 2.4.

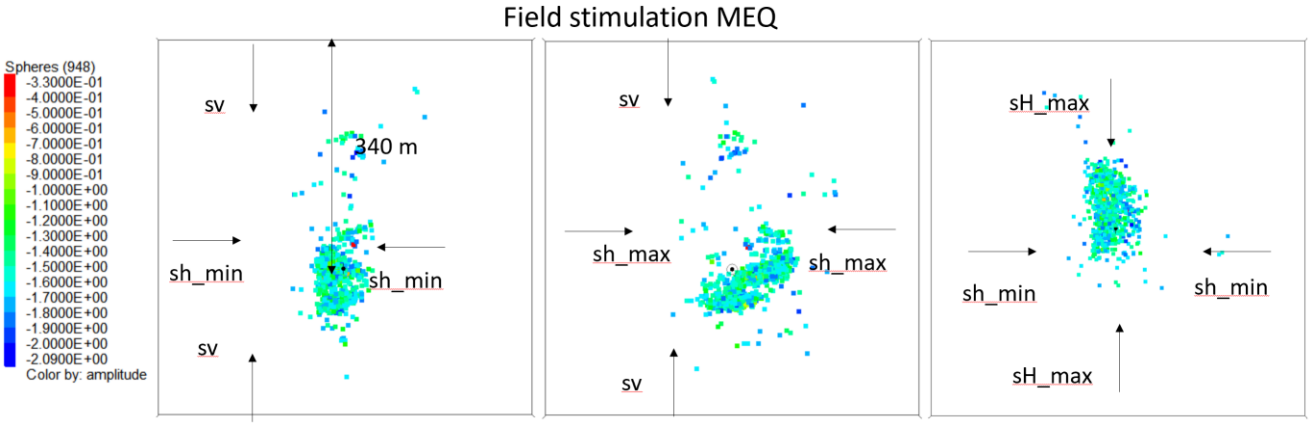

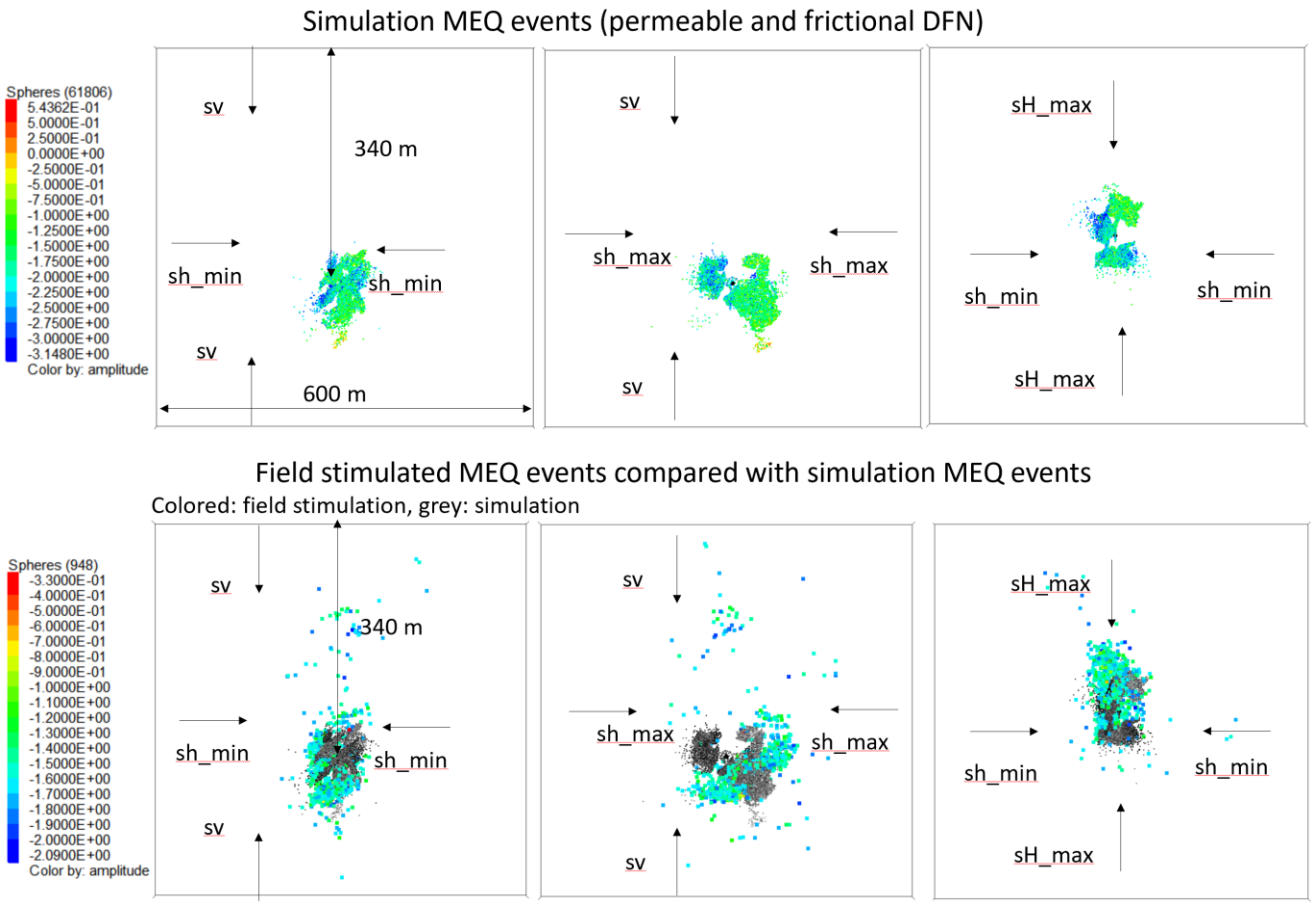

Figure 11: Comparison of the field detected microseismicity cloud with simulation results for Stage 2. Field detected maximum magnitude is -0.33, and simulation maximum magnitude is 0.54.

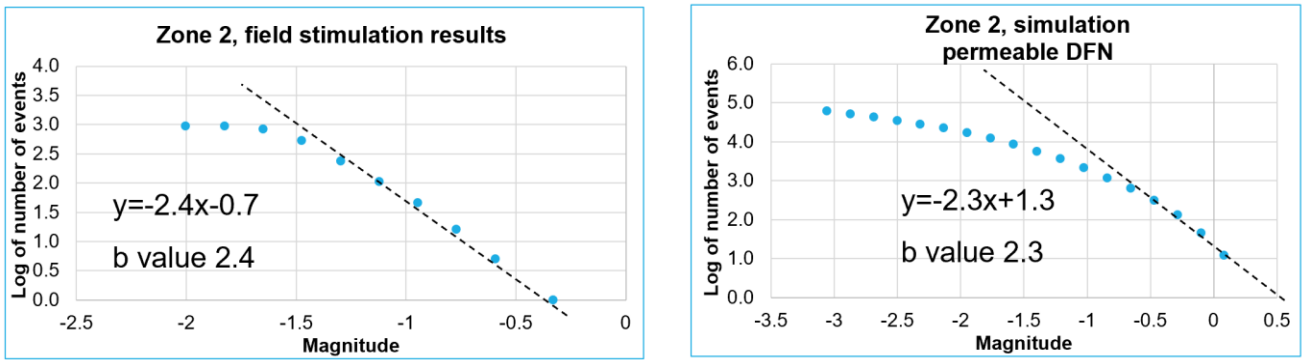

Figure 12: Comparison of the field detected microseismicity b-value with simulation results for Stage 2.

4.3 Stage 3

Figure 13 shows the comparison of the microseismicity events generated in the numerical model and detected in the field for Stage 3. The microseismic events extent from the model matches the field data. The number of events from the numerical model is much larger than the field data. As it is shown in Figure 14, the field geophones cannot detect the microseismicity magnitude smaller than – 1.7, but the magnitude can be as low as – 2.5 in the model. The b value of the numerical model is 2.3, which is close to the b value of the field data, 2.2.

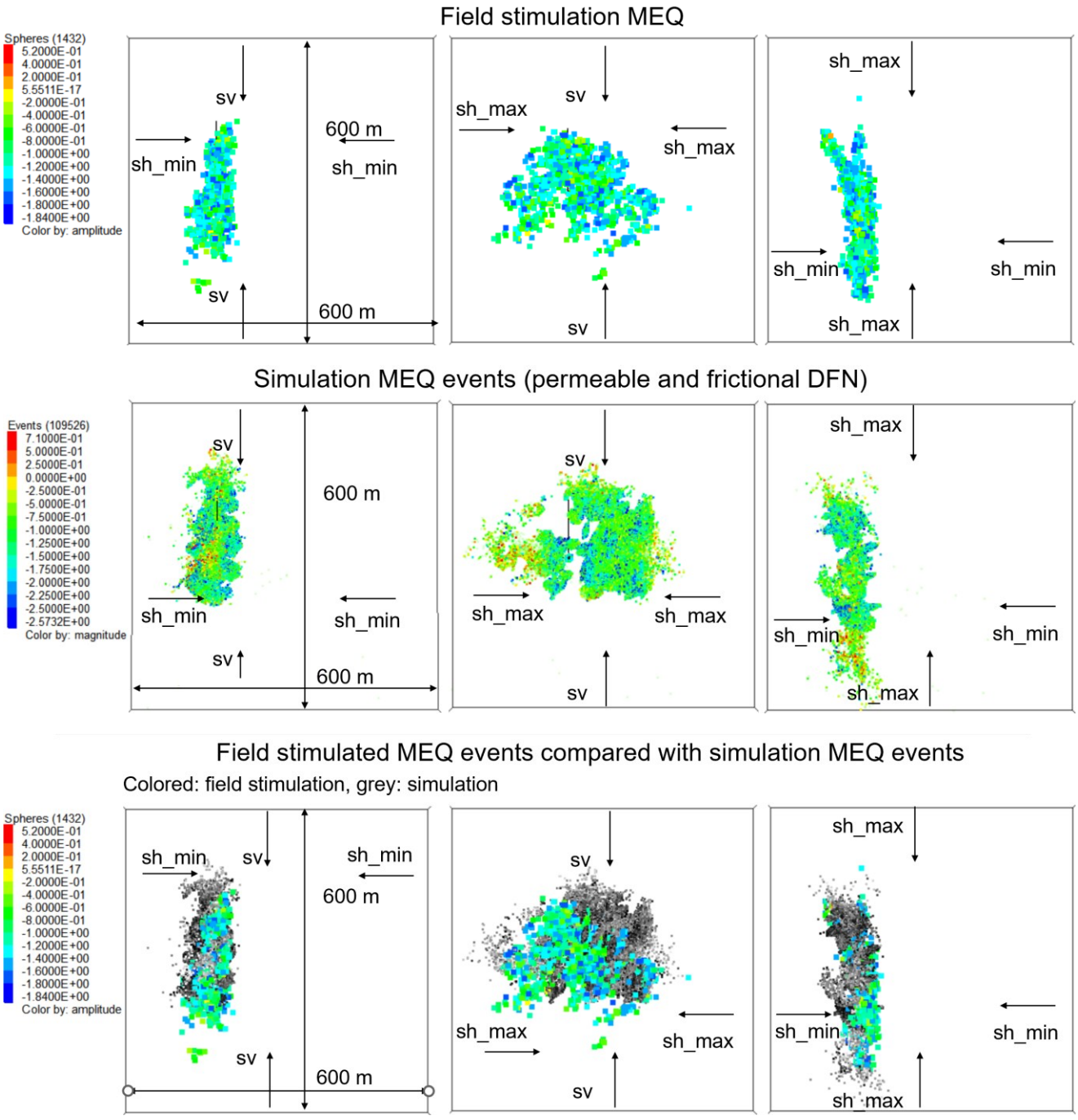

Figure 13: Comparison of the field detected microseismicity cloud with simulation results for Stage 3. Field detected maximum magnitude is 0.52, and simulation maximum magnitude is 0.71.

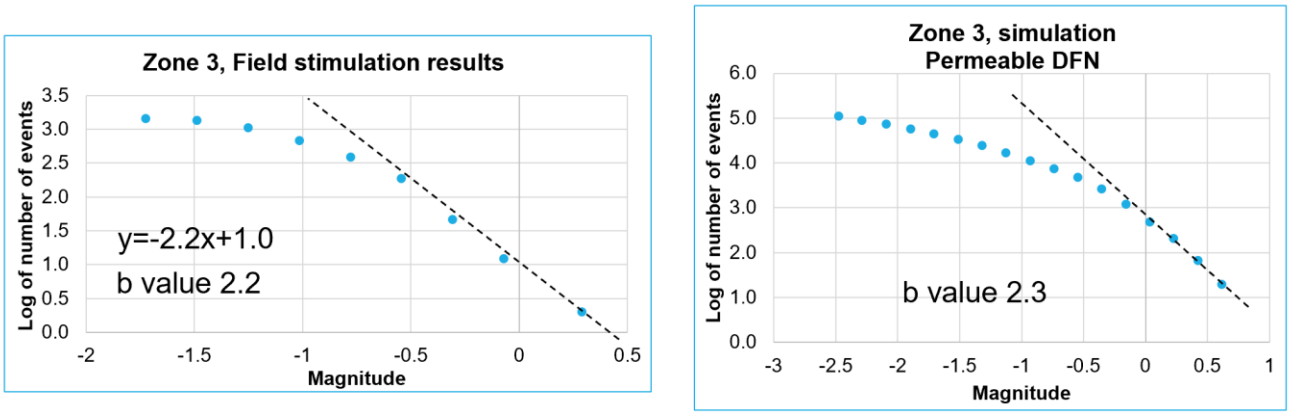

Figure 14: Comparison of the field detected microseismicity b-value with simulation results for Stage 3. Weak and initial permeable DFN.

4.4 Summary

For all the three stages, the extents of microseismicity events from the numerical model match those from the field. Stage 1 was conducted at a 200 ft openhole section, and there are large uncertainties in the fracture initiation location. Also, the planned injection point is different from the actual perforation location for Stages 2 and 3. Therefore, the goal of the comparison is not to match the exact locations of the microseismic events but to match the extent of the cloud of events.

The b value of the filed data for all the three stages ranges from 2.2 to 2.4. The b value from the numerical models also ranges from 2.3 to 2.4. This indicates that the numerical models well represent the mechanism in the field.

The height of microseismicity cloud of Stage 3 is much larger than that of Stage 1 and Stage 2. The reason is that the Stage 3 is hydraulic fracture dominated due to large fluid viscosity while for Stages 1 and 2 fluid leakoff into DFN is dominant.

5. CONCLUSIONS

The numerical models for three stages use the same DFN geometrical realization and DFN strength. The DFN fractures in the models are assumed to have 37° friction angle, zero cohesion and zero tensile strength. The numerical models predict that rock response to stimulation by fluid injection in all three stages includes combination of hydraulic fracturing and stimulation of DFN. DFN leakoff seems to dominate response in Stages 1 and 2, which is expected considering use of slick water. Stage 3, which was stimulated with xlink fluid, is dominated by hydraulic fracturing.

For Stage 1, the simulated net pressure matches well the field data. For Stages 2 and 3, the simulated net pressure matches the field data at later injection times (greater than 80 minutes). Injection pressure histories (for these stages that use cased completion with perforation clusters) are not matched well in early period probably because of complex evolving geometries and processes in well near field that are not included in this model.

The extents of the simulated microseismicity events and b value match the field recorded data for all the three stages. Stage 3 has the largest height of microseismic cloud due to large fluid viscosity.

ACKNOWLEDGEMENTS

Funding for this work was provided by the U.S. DOE under grant DE-EE0007080 “Enhanced Geothermal System Concept Testing and Development at the Milford City, Utah FORGE Site.” We thank the many stakeholders who are supporting this project, including Smithfield, Utah School and Institutional Trust Lands Administration, and Beaver County, as well as the Utah Governor’s Office of Energy Development.

This research made use of the resources of the High Performance Computing Center at Idaho National Laboratory, which is supported by the Office of Nuclear Energy of the U.S. Department of Energy and the Nuclear Science User Facilities under Contract No. DE-AC07-05ID14517.

REFERENCES

Finnila, A., Doe, T., Podgorney, R., Damjanac, B., and Xing, P. Revisions to the Discrete Fracture Network Model at Utah FORGE Site, GRC Transactions, Vol. 45, (2021).

Itasca Consulting Group, Inc. XSite (Version 3.0.48). Minneapolis: Itasca, (2020).

McLennan, J., England, K., Rose, P., Moore, J., and Barker, B. Stimulation of a High-Temperature Granitic Reservoir at the Utah FORGE Site, Proceedings, SPE Hydraulic Fracturing Technology Conference and Exhibition, The Woodlands, Texas (2023).

Xing, P., Winkler, D., Swearingen, L., Moore J., and J. McLennan. In-Situ Stresses and Permeability Measurements from Testings in Injection Well 16A(78)-32 at Utah FORGE Site, GRC Transactions, Vol. 45, (2021).

Xing, P., Damjanac, B., Radakovic-Guzina, Z., Maurilio, T., Finnila, A., Podgorney, R., Moore J., and J. McLennan. Numerical Simulation of Injection Tests at Utah FORGE Site, GRC Transactions, Vol. 46, (2022).